

## Probing Positron Cooling in Noble Gases via Annihilation $\gamma$ Spectra

D. G. Green\*

*Centre for Theoretical Atomic, Molecular and Optical Physics, School of Mathematics and Physics,  
Queen's University Belfast, Belfast BT7 1NN, Northern Ireland, United Kingdom*

(Received 15 June 2017; published 16 November 2017)

$\gamma$  spectra for positron annihilation in noble-gas atoms are calculated using many-body theory for positron momenta up to the positronium-formation threshold. These data are used, together with time-evolving positron-momentum distributions determined in the preceding Letter [Phys. Rev. Lett. **119**, 203403 (2017)], to calculate the time-varying  $\gamma$  spectra produced during positron cooling in noble gases. The  $\gamma$  spectra and their  $\bar{S}$  and  $\bar{W}$  shape parameters are shown to be sensitive probes of the time evolution of the positron momentum distribution and thus provide a means of studying positron cooling that is complementary to positron lifetime spectroscopy.

DOI: 10.1103/PhysRevLett.119.203404

Low-energy positrons annihilate with atomic electrons forming two  $\gamma$  rays whose Doppler-broadened energy spectra are characteristic of the electron state involved; e.g., annihilation on tightly bound core electrons contributes to the high-Doppler-shift wings of the spectrum [1]. This gives positrons important use in, e.g., studies of surfaces, defects, and porosity of industrially important materials [2–5]. Importantly, the  $\gamma$  spectra are also characteristic of the positron momentum at the instant of annihilation: increased positron momentum results in an increased annihilating-pair momentum and larger  $\gamma$ -ray Doppler shifts. Measurement of the time-varying  $\gamma$  spectra, or so-called AMOC (“age momentum correlation”) spectra [6–10], in which the positron “age” (lifetime from source to annihilation) and  $\gamma$  spectra are measured in coincidence, can thus enable the study of positron and positronium cooling in atomic gases [11,12]. Understanding the dynamics of positron cooling in gases is critical for the accurate interpretation of experiments, and for the development of efficient positron cooling in traps and accumulators [13] and a cryogenically cooled, ultrahigh-energy-resolution, trap-based positron beam [14,15].

Positron cooling in atomic gases has traditionally been probed by positron annihilation lifetime spectroscopy (PALS) [16,17]. The dynamics of positron cooling in noble gases was elucidated in the preceding Letter Ref. [18], where Monte Carlo (MC) simulations based on accurate scattering and annihilation cross sections calculated using many-body theory (MBT) were used to determine the time-evolving positron momentum distribution and normalized annihilation rate  $\bar{Z}_{\text{eff}}(t)$ . That work found that a strikingly small fraction of initial positrons survive to thermalization, affecting the measured annihilation rate and explaining the discrepancy between trap-based [19] and gas-cell [20] measurements in Xe. Overall, good agreement was found with the long-standing PALS measurements for all the atoms except Ne, for which the calculated cooling time was found to be drastically longer than the measured value. It

was proffered that the discrepancy was due to an incorrect analysis of the experimental data and/or the presence of impurities. New experiments are called for to further test the theoretical results. Verifying the accuracy of the calculations is important to ensure that the complicated positron-atom many-body system is well understood.

In this Letter, we use MBT to investigate the dependence of the positron annihilation  $\gamma$  spectra for the noble-gas atoms on the positron momentum up to the positronium (Ps) formation threshold, and demonstrate that the time-varying  $\gamma$  spectra provide a sensitive probe of positron cooling in noble gases that is complementary to PALS. The MBT takes full account of positron-atom and positron-electron correlations, including virtual-positronium formation [1,21–23]. [Note that for condensed matter such correlations can also be described using quantum Monte Carlo and density functional theory methods (see, e.g., [24,25]).] Specifically, we extend the calculations of Ref. [1], where  $\gamma$  spectra for thermal positron annihilation with individual core and valence subshells of the noble gases were calculated using MBT. It provided an accurate description of the measured spectra for Ar, Kr, and Xe and firmly established the relative contributions of various atomic orbitals to the spectra. Using the spectra calculated at all positron momenta, together with the time-evolving positron-momentum distributions calculated using MBT-based MC simulations in Ref. [18], we calculate the  $\gamma$  spectra produced during positron cooling. We analyze the dynamics of the  $\bar{S}$  and  $\bar{W}$  shape parameters, which characterize the low and high (two- $\gamma$ ) momentum parts of the spectra, during the process of positron thermalization. The present results provide benchmarks to which positron-cooling experiments can compare.

*Many-body theory calculations of annihilation  $\gamma$  spectra.*—In the dominant process, a positron of momentum  $\mathbf{k}$  and energy  $\varepsilon = k^2/2$  annihilates with an electron in state  $n$  to form two  $\gamma$ -ray photons of total momentum  $\mathbf{P}$  [26]. In the center-of-mass frame the two  $\gamma$  rays have equal energies

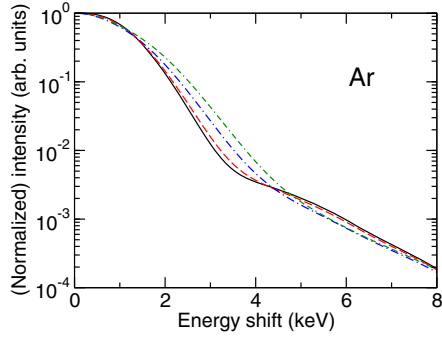


FIG. 1.  $\gamma$  spectra  $w_k(\epsilon)$  (normalised to unity at  $\epsilon = 0$ ) for annihilation in Ar, for positrons of momenta  $k = 0.04$  a.u. (solid line),  $k = 0.2$  a.u. (dashed line),  $k = 0.4$  a.u. (dashed-dotted line), and  $k = 0.6$  a.u. (dash-dash-dotted line).

$mc^2 = 511$  keV (neglecting the initial positron and electron energies). In the laboratory frame the photon energies are Doppler shifted by  $\epsilon \leq Pc/2$ , and their spectrum is [1,27]

$$w_{nk}(\epsilon) = \frac{1}{c} \int_{2|e|/c}^{\infty} \int_{\Omega_{\mathbf{P}}} |A_{ne}(\mathbf{P})|^2 \frac{d\Omega_{\mathbf{P}}}{(2\pi)^3} P dP, \quad (1)$$

where  $A_{ne}(\mathbf{P})$  is the annihilation amplitude. It is calculated via a diagrammatic expansion (see Fig. 1 of Ref. [1]), including the zeroth-order vertex, and the first- and higher-order (“ $\Gamma$ -block”) corrections, which account for the attractive electron-positron interaction at short range [1,27,28]. The total spectrum is given by the sum over all (occupied) electron states  $n$ :  $w_k(\epsilon) = \sum_n w_{nk}(\epsilon)$ . Its integral gives the effective annihilation rate  $Z_{\text{eff}}(k) = \int_{-\infty}^{\infty} w_k(\epsilon) d\epsilon$  [1,27,29,30].

To illustrate the momentum dependence of the shape of the  $\gamma$  spectra, Fig. 1 shows the MBT-calculated  $\gamma$  spectra for argon, for  $k = 0.04$ – $0.6$  a.u., normalized to unity at zero energy shift. The calculations included  $s$ -,  $p$ -, and  $d$ -wave incident positrons (higher partial waves contribute negligibly) [31] annihilating on the valence  $ns$  and  $np$  and subvalence  $(n-1)s$ ,  $(n-1)p$ , and  $(n-1)d$  subshells, e.g., in Ar, the  $3s$  and  $3p$  valence and  $2s$  and  $2p$  subshells. In general, at a given positron momentum, the spectra are characteristic of the electron orbitals involved; e.g., annihilation with core electrons produces a broader component than that with valence electrons, contributing to the distinct shoulders in the spectrum [1]. The figure shows that the  $\gamma$  spectrum is significantly broadened for higher positron momenta (see also Fig. 20 of Ref. [32]). Increasing the positron momentum leads to increased momenta of the annihilating electron-positron pair and allows the positron to penetrate deeper into the atomic core, ultimately resulting in larger Doppler shifts. The exact shape of the spectra is somewhat complicated. As  $k$  increases, the broadening of the core and valence contributions is accompanied by the increasing relative importance of  $p$ - and  $d$ -wave

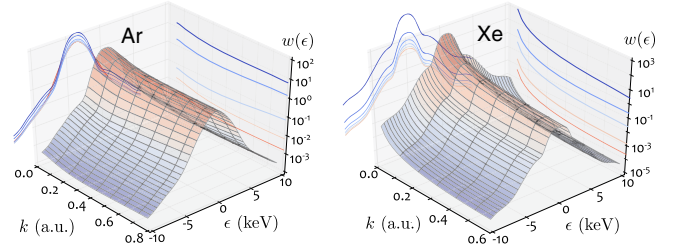


FIG. 2.  $\gamma$  spectra  $w_k(\epsilon)$  for positron annihilation in Ar and Xe as a function of positron momentum  $k$  up to the positronium-formation threshold. Also shown are projections at Doppler-shifted energies  $\epsilon = 0, 2, 4, 6,$  and  $8$  keV and at  $k = 0.02$  a.u. and from  $k = 0.1$  in step sizes of  $0.1$  a.u.

contributions, whose spectra are typically narrower than the  $s$ -wave one [28,33].

Figure 2 shows the absolute MBT-calculated  $\gamma$  spectra for Ar and Xe as illustrative examples. The increase in magnitude of the spectra as  $k \rightarrow 0$  accords with the rise of the effective annihilation rate  $Z_{\text{eff}}(k)$  (see Fig. 16 in Ref. [23]). This effect is due to the existence of positron-atom virtual levels [35], signified by large scattering lengths (see Table I in Ref. [23]).

The momentum dependence of the spectra can be characterized through the dimensionless parameters  $W(k) = 2Z_{\text{eff}}(k)^{-1} \int_{\epsilon_W}^{\infty} w_k(\epsilon) d\epsilon$  and  $S(k) = 2Z_{\text{eff}}(k)^{-1} \int_0^{\epsilon_S} w_k(\epsilon) d\epsilon$ , where  $\epsilon_W$  and  $\epsilon_S$  are constants.  $W$  parameterizes the high (two- $\gamma$ ) momentum “wing” part of the spectrum, which originates from annihilation with core electrons and with valence electrons when they have larger momenta at smaller, core radii.  $S$  parameterizes the low two- $\gamma$ -momentum region of the spectrum, which originates predominantly from annihilation on valence electrons. Figure 3 shows the calculated  $W(k)$  for He to Xe for the raw  $\gamma$  spectra and that convolved with the typical Ge detector-resolution function  $D(\epsilon) = N \exp[-(\epsilon/a\Delta E)^2]$ , where  $a = 1/(4 \ln 2)^{1/2}$ ,  $N = (a\Delta E\sqrt{\pi})^{-1}$  is a normalization constant,

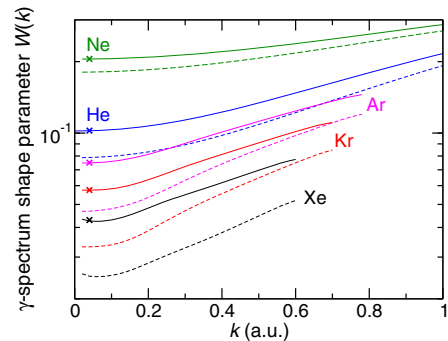


FIG. 3. The shape parameter  $W(k)$  (see the text) for raw (dashed line) and detector-convolved  $\gamma$  spectra (solid line) for positron annihilation in He (blue), Ne (green), Ar (magenta), Kr (red), and Xe (black). Crosses mark the values for the thermally averaged (at  $T = 293$  K) detector-convolved spectra.

and  $\Delta E = 1.16$  keV [36], with  $\epsilon_W = 2.0$  keV. It is clear that  $W(k)$  is sensitive to the positron momentum, increasing monotonically with  $k$  by a factor of 1.5–2 up to the Ps-formation threshold for all the noble gases considered. It decreases across the sequence Ne to Xe (He is an exception, since it has no core electrons). In contrast, the probability of annihilation on core electrons  $P_{\text{core}} = Z_{\text{eff}}^{\text{core}}/Z_{\text{eff}}$ , where  $Z_{\text{eff}}^{\text{core}}$  is the annihilation rate on the core subshells, is found to increase from Ne to Xe and decrease with positron momentum [28]. Thus, the momentum dependence of  $W(k)$  is dominated by the contribution of the positron momentum itself rather than the change in the relative core annihilation probability.

*Positron cooling probed via time-varying  $\gamma$  spectra.*— The time-varying  $\gamma$  spectrum produced by positrons cooling in gases is  $\bar{w}_\tau(\epsilon) = \int_0^\infty f(k, \tau) w_k(\epsilon) dk$ , where  $\tau$  is the time (typically quoted in nanoseconds) scaled by the number density of the gas (in amagat):  $\tau = nt$ , and  $f(k, \tau)$  is the positron momentum-space distribution. It is normalized as  $\int_0^\infty f(k, \tau) dk = F(\tau)$ , the fraction of initial positrons remaining. The momentum distributions  $f(k, \tau)$  for positron cooling in noble gases were calculated recently in Ref. [18] via MC simulations based on the accurate MBT cross sections. There it was shown that, for all the noble gases, positrons rapidly bunch around the minimum in the coefficient  $B(k) = k\sigma_i k_B T m/M$ , where  $\sigma_i$  is the momentum-transfer cross section (see Fig. 1 of Ref. [18]), where the cooling rate slows, making the overall cooling times somewhat insensitive to the exact form of the initial distribution. After bunching in the minima, the positrons cool further slowly, before evolving towards the steady-state distribution (the Maxwell Boltzmann distribution for He to Kr, but not for Xe, see Ref. [18] and below). The characteristic trajectory followed by the positrons in  $(k, \tau)$  space, along with the dependence of the  $\gamma$  spectra on the positron momentum, leads to a characteristic AMOC spectrum, i.e., the number of  $\gamma$  rays  $\tilde{N}_\gamma$  (per unit positron) detected per unit time and Doppler-shifted energy. It can be measured in experiments [6–10,12] and calculated as  $d^2\tilde{N}_\gamma/d\tau d\epsilon = 2\pi r_0^2 c F(\tau) \bar{w}_\tau(\epsilon)$ . Integrating over the Doppler-shifted energy  $\epsilon$  gives the lifetime spectrum (normalized to one positron)  $A(\tau) = d\tilde{N}_\gamma/2d\tau = -dF(\tau)/d\tau = \pi r_0^2 c F(\tau) \int_{-\infty}^\infty \bar{w}_\tau(\epsilon) d\epsilon = \pi r_0^2 c F(\tau) \bar{Z}_{\text{eff}}(\tau)$  [37] that is traditionally measured in PALS [16,17].

An example AMOC spectrum is shown in Fig. 4 for Ar (cf. Fig. 2 in Ref. [18]), calculated using the detector-convolved spectra for positrons initially distributed uniformly in energy up to the Ps-formation threshold (see Supplemental Material [38] for corresponding plots for the noble gases He to Xe). The overall decrease in the magnitude of the spectra in time is due to the reduction in the number of positrons surviving  $F(\tau)$  (see Fig. 3 in Ref. [18]) dominating over the increase in  $w_k$  as  $k \rightarrow 0$ . The flattening of the “ridge” at  $\tau \lesssim 200$  ns amg occurs as

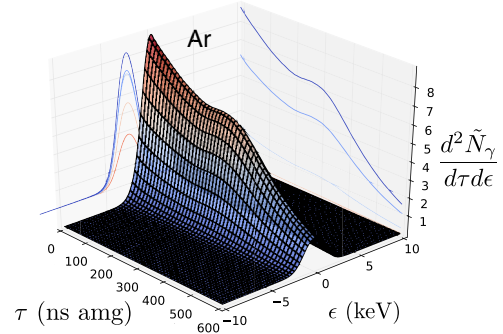


FIG. 4. AMOC spectrum (number of  $\gamma$  rays detected per unit time and Doppler-shifted energy) for Ar, in units of  $\pi r_0^2 c$ , calculated using the detector-convolved spectra  $\bar{w}_\tau(\epsilon)$ , with positrons initially distributed uniformly in energy. Also shown are projections at  $\tau = 100, 200, 300, 400,$  and  $500$  ns and  $\epsilon = 0, 1, 2, 3, 4,$  and  $5$  keV.

the positrons are “trapped” around the momentum-transfer cross section minima and cool slowly through it. Beyond  $\tau \sim 200$ – $300$  ns amg, epithermal annihilation occurs at momenta below the momentum-transfer cross-section minimum. Integrating over  $\epsilon$ , this “knee” in the spectrum becomes the characteristic shoulder region observed in the lifetime spectrum [39–41]. It is known to be relatively insensitive to the initial positron momentum distribution [16,42]. At later time-densities ( $\tau > 400$  ns amg), the AMOC spectrum is proportional to  $F(\tau)w_\infty$ , where  $w_\infty = \int_0^\infty w_k(\epsilon) f_\infty(k) dk$  and  $f_\infty(k)$  is the final quasi-steady-state positron-momentum distribution [43].

From the AMOC spectrum, the time-varying  $\gamma$ -spectrum shape parameters  $\bar{W}(\tau) \equiv 2\bar{Z}_{\text{eff}}(\tau)^{-1} \int_{\epsilon_W}^\infty \bar{w}_\tau(\epsilon) d\epsilon$  and  $\bar{S}(\tau) \equiv 2\bar{Z}_{\text{eff}}(\tau)^{-1} \int_0^{\epsilon_S} \bar{w}_\tau(\epsilon) d\epsilon$  can be determined. Figure 5(a) shows the calculated  $\bar{S}(\tau)$  for Ar compared with the recent experimental result [12] (obtained using  $\epsilon_S = 0.5$  keV). Although the theoretical value is systematically lower than the measured one, the time dependence is in near perfect agreement. This is made evident by scaling the theoretical result as  $\bar{S}_{\text{sc}} = 1.43\bar{S} - 0.13$ . Such a scaling can account for effects in background subtraction in the experiment: e.g., calculating  $\bar{S}(\tau)$  by first subtracting  $0.1$  (ns amg keV) $^{-1}$  from the spectrum produces excellent agreement with the experiment (green dashed-dotted line). In PALS, a common measure of the cooling time is the “shoulder length”  $\tau_s$ , defined via  $\bar{Z}_{\text{eff}}(\tau_s) = \bar{Z}_{\text{eff}} - 0.1\Delta Z$ , where  $\bar{Z}_{\text{eff}}$  is the final steady-state effective annihilation rate and  $\Delta Z \equiv \bar{Z}_{\text{eff}} - \bar{Z}_{\text{min}}$ , where  $\bar{Z}_{\text{min}}$  is the minimum of  $\bar{Z}_{\text{eff}}(\tau)$  [16,17,45]. An alternative measure is the “complete thermalization time,” defined as the time-density at which the root-mean-square momentum of the positron distribution is within 1% of the thermal value  $k_{\text{th}} \sim 0.0526$  for a gas at  $T = 293$  K. The figure shows that  $\bar{S}$  reaches its steady-state value close to the shoulder time, impressively

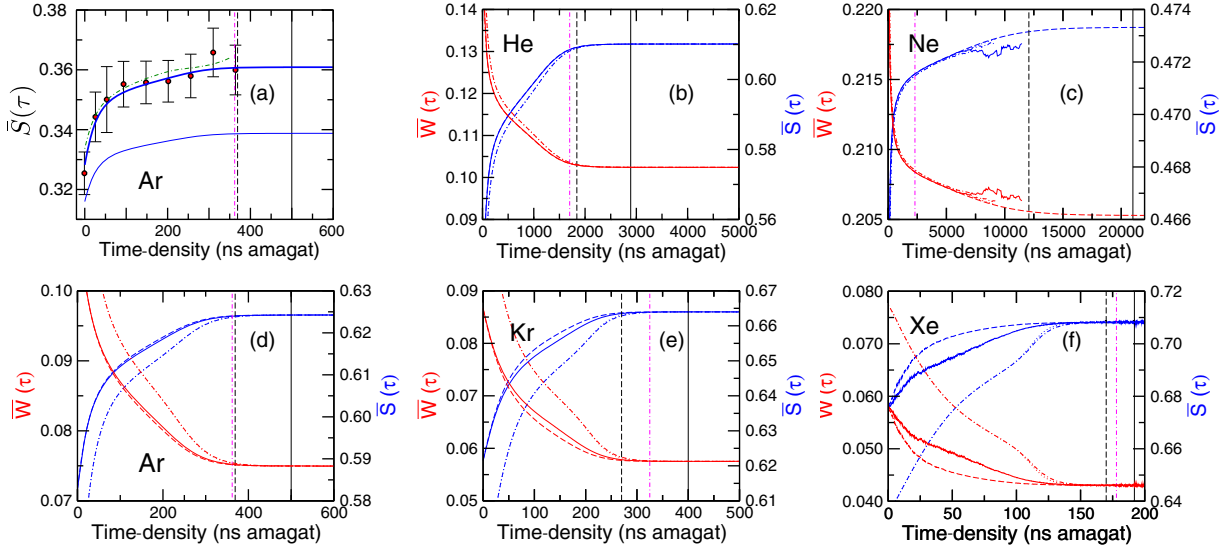


FIG. 5. (a)  $\bar{S}(\tau)$  for Ar: experiment [12] (red circles); present calculation, for positrons distributed uniformly in energy (thin solid line); that scaled as  $\bar{S}_{sc} = 1.43\bar{S} - 0.13$  (thick solid line); and calculated by first subtracting  $0.1 \text{ keV}^{-1}$  from  $\bar{w}_\tau(\epsilon)$  (green dashed-dotted line). Also marked are the calculated [18] and measured [44] shoulder lengths (vertical dot-dashed and dashed lines, respectively) and calculated complete thermalization time (solid vertical line) [18]; (b)–(f)  $\bar{W}(\tau)$  (red) and  $\bar{S}(\tau)$  (blue) parameters for detector-convolved  $\gamma$  spectra: excluding and including the depletion of the distribution due to annihilation, for positrons initially distributed uniformly in energy (dashed and solid lines) and with the energy equal to the Ps-formation threshold (dotted and dash-dotted lines, which are almost indistinguishable). Also shown are the shoulder lengths and thermalization times calculated in Ref. [18] (dashed and solid vertical lines) and the experimental shoulder lengths of Refs. [44] (He and Ne) and [20] (Ar, Kr and Xe) (dash-dotted vertical line). The steady-state values of  $\bar{W}$  ( $\bar{S}$ ) are He, 0.102 (0.610); Ne, 0.2067 (0.473); Ar, 0.624 (0.075); Kr, 0.664 (0.058); and Xe, 0.708 (0.043). The value for Ne neglected the depletion of the distribution due to annihilation. For Ne, at  $\tau \sim 5000 \text{ ns amg}$ , where  $F(\tau) \lesssim 10^{-2}$ ,  $W(\tau) = 0.2073$  and  $S(\tau) = 0.472$ .

demonstrating how the spectra can be used to probe positron cooling times.

Figures 5(b)–5(f) show  $\bar{W}(\tau)$  and  $\bar{S}(\tau)$  for He to Xe (obtained with  $\epsilon_W = 2.0$  and  $\epsilon_S = 1.0 \text{ keV}$ ) calculated using the detector-convolved spectra excluding and including depletion of the positron distribution due to annihilation, for positrons initially distributed either uniformly in energy or with energy equal to the Ps-formation threshold [46]. Also marked are the experimental shoulder lengths  $\tau_s$  [20,44] and calculated  $\tau_s$ , and complete thermalization times from Ref. [18]. In general, as the positrons cool, the annihilation spectrum becomes narrower, so the  $\bar{S}$  parameter increases and the  $\bar{W}$  parameter decreases with time, before reaching a steady-state value at thermalization. For lighter atoms (He and Ne), the initial positron energy distribution (i.e., uniform vs monoenergetic) does not play much of a role. Also, for these atoms the annihilation rate remains much smaller than the cooling rates at all times. As a result, the depletion of positrons during the cooling process does not affect the time dependence of the  $\gamma$  spectra. For Ne, the fraction of positrons that survive beyond  $\tau \sim 8000 \text{ ns amg}$  is practically zero (leading to poor statistics), owing to positrons becoming trapped in the deep momentum-transfer minimum, where cooling is slow [18]. Given the insensitivity to the initial distribution, accurate measurements of  $\bar{W}$  and

$\bar{S}$  could confirm the theoretical predictions. In contrast, for Ar, Kr, and Xe, the initial positron distribution has a sizable effect on the time evolution of the spectra. The more physical uniform-energy distribution leads to fast evolution of  $\bar{S}$  and  $\bar{W}$  at earlier times towards the final “thermalized” values. For these atoms, the information provided by AMOC measurements, combined with theoretical studies, could enable the determination of the form of the initial distributions, about which little is currently known. On the other hand, the effect of positron depletion slows down the time evolution of  $\bar{S}$  and  $\bar{W}$ , which is particularly noticeable in Xe. In this system, the rate of positron annihilation competes strongly with that of positron cooling. Because of the strong peaking of  $Z_{\text{eff}}(k)$  at small  $k$ , annihilation effectively removes the slowest positrons, impeding thermalization [and, in fact, leading to a non-Maxwell-Boltzmann asymptotic momentum distribution  $f_\infty(k)$ ] [18].

*Summary.*—Many-body-theory-based calculations of time-varying  $\gamma$  spectra for positron annihilation on noble gases have been presented. The benchmark results demonstrate that the spectra provide a sensitive probe of positron cooling, which is complementary to positron lifetime spectroscopy.

Data relating to this article can be accessed online [47].

D. G. G. thanks Gleb Gribakin for insightful discussions and useful comments on the manuscript. D. G. G. is supported by the United Kingdom Engineering and Physical Sciences Research Council, Grant No. EP/N007948/1.

\*d.green@qub.ac.uk

- [1] D. G. Green and G. F. Gribakin, *Phys. Rev. Lett.* **114**, 093201 (2015).
- [2] P. J. Schultz and K. G. Lynn, *Rev. Mod. Phys.* **60**, 701 (1988).
- [3] M. J. Puska and R. M. Nieminen, *Rev. Mod. Phys.* **66**, 841 (1994).
- [4] F. Tuomisto and I. Makkonen, *Rev. Mod. Phys.* **85**, 1583 (2013).
- [5] C. Hugenschmidt, *Surf. Sci. Rep.* **71**, 547 (2016).
- [6] H. Stoll, K. M. M. Koch, and J. Major, *Nucl. Instrum. Methods Phys. Res., Sect. B* **56–57**, 582 (1991).
- [7] *Positron Beams and Their Applications*, edited by P. Coleman (World Scientific, Singapore, 2000).
- [8] A. Siegle, H. Stoll, P. Castellaz, J. Major, H. Schneider, and A. Seeger, *Appl. Surf. Sci.* **116**, 140 (1997).
- [9] J. Engbrecht, *Nucl. Instrum. Methods Phys. Res., Sect. B* **221**, 119 (2004).
- [10] U. Ackermann, B. Löwe, M. Dickmann, J. Mitteneder, P. Sperr, W. Egger, M. Reiner, and G. Dollinger, *New J. Phys.* **18**, 113030 (2016).
- [11] J. J. Engbrecht, M. J. Erickson, C. P. Johnson, A. J. Kolan, A. E. Legard, S. P. Lund, M. J. Nyflot, and J. D. Paulsen, *Phys. Rev. A* **77**, 012711 (2008).
- [12] Y. Sano, Y. Kino, T. Oka, and T. Sekine, *JJAP Conf. Proc.* **2**, 011004 (2014).
- [13] I. Al-Qaradawi, M. Charlton, I. Borozan, R. Whitehead, and I. Borozan, *J. Phys. B* **33**, 2725 (2000).
- [14] M. R. Natisin, J. R. Danielson, and C. M. Surko, *J. Phys. B* **47**, 225209 (2014).
- [15] M. R. Natisin, J. R. Danielson, and C. M. Surko, *Appl. Phys. Lett.* **108**, 024102 (2016).
- [16] T. C. Griffith and G. R. Heyland, *Phys. Rep.* **39**, 169 (1978).
- [17] M. Charlton, *Rep. Prog. Phys.* **48**, 737 (1985).
- [18] D. G. Green, preceding Letter, *Phys. Rev. Lett.* **119**, 203403 (2017).
- [19] T. J. Murphy and C. M. Surko, *J. Phys. B* **23**, L727 (1990).
- [20] G. L. Wright, M. Charlton, T. C. Griffith, and G. R. Heyland, *J. Phys. B* **18**, 4327 (1985).
- [21] V. A. Dzuba, V. V. Flambaum, W. A. King, B. N. Miller, and O. P. Sushkov, *Phys. Scripta* **T46**, 248 (1993).
- [22] V. A. Dzuba, V. V. Flambaum, G. F. Gribakin, and W. A. King, *J. Phys. B* **29**, 3151 (1996).
- [23] D. G. Green, J. A. Ludlow, and G. F. Gribakin, *Phys. Rev. A* **90**, 032712 (2014).
- [24] N. D. Drummond, P. López Ríos, R. J. Needs, and C. J. Pickard, *Phys. Rev. Lett.* **107**, 207402 (2011).
- [25] B. Barbiellini and J. Kuriplach, *Phys. Rev. Lett.* **114**, 147401 (2015).
- [26] V. B. Berestetskii, E. M. Lifshitz, and L. P. Pitaevskii, *Quantum Electrodynamics*, 2nd ed. (Pergamon, Oxford, 1982).
- [27] L. J. M. Dunlop and G. F. Gribakin, *J. Phys. B* **39**, 1647 (2006).
- [28] D. G. Green and G. F. Gribakin, [arXiv:1502.08045](https://arxiv.org/abs/1502.08045).
- [29] P. A. Fraser, *Adv. At. Mol. Phys.* **4**, 63 (1968).
- [30] I. Pomeranchuk, *Zh. Eksp. Teor. Fiz.* **19**, 183 (1949).
- [31] After integrating over the directions of  $\mathbf{P}$ , all positron partial waves contribute to the amplitude incoherently, such that it can be calculated independently for each.
- [32] D. G. Green and G. F. Gribakin, *Phys. Rev. A* **88**, 032708 (2013).
- [33] At low momenta, the partial rate  $Z_{\text{eff}}^{(\ell_e)}(k) \sim k^{2\ell_e}$  [34] and the  $s$ -wave contribution dominates the spectra. However, the contribution of  $p$  and  $d$  waves increases and becomes comparable at positron momenta close to the positronium-formation threshold.
- [34] L. D. Landau and E. M. Lifshitz, *Quantum Mechanics (Non-relativistic Theory)*, 3rd ed., Course of Theoretical Physics Vol. 3 (Pergamon, Oxford, 1977).
- [35] V. I. Goldanskii and Y. S. Sayasov, *Phys. Lett.* **13**, 300 (1964).
- [36] K. Iwata, G. F. Gribakin, R. G. Greaves, and C. M. Surko, *Phys. Rev. Lett.* **79**, 39 (1997).
- [37] This holds for a spectrum convolved with a detector-resolution function  $D(\epsilon)$  normalized as  $\int_{-\infty}^{\infty} D(\epsilon) d\epsilon = 1$ .
- [38] See Supplemental Material at <http://link.aps.org/supplemental/10.1103/PhysRevLett.119.203404> for additional figures showing the  $\gamma$  spectra as a function of positron momentum, and the time-varying  $\gamma$  spectra during cooling, for He, Ne, Ar, Kr and Xe.
- [39] W. R. Falk and G. Jones, *Can. J. Phys.* **42**, 1751 (1964).
- [40] S. J. Tao, J. Bell, and J. H. Green, *Proc. Phys. Soc. London* **83**, 453 (1964).
- [41] D. A. L. Paul, *Proc. Phys. Soc. London* **84**, 563 (1964).
- [42] A. Farazdel and I. R. Epstein, *Phys. Rev. A* **16**, 518 (1977).
- [43] For He, the final distribution is the Maxwell-Boltzmann distribution. For the heavier gases, most notably Xe, the low-momentum side of the final distribution is suppressed relative to the Maxwell-Boltzmann distribution. This is a result of the rapid depletion of low-momentum positrons due to the vigorous increase in  $Z_{\text{eff}}$  at low momenta.
- [44] P. G. Coleman, T. C. Griffith, G. R. Heyland, and T. L. Killeen, *J. Phys. B* **8**, 1734 (1975).
- [45] D. A. L. Paul and C. Y. Leung, *Can. J. Phys.* **46**, 2779 (1968).
- [46] The initial distribution of constant energy is unphysical but provides an upper limit on the cooling times.
- [47] <http://doi.org/10.17034/9da6ab49-3a41-4042-90ed-f7e479d2f437>.